Volume 40, Number 15, 2007 ISSN 0021-9290

ELSEVIER

Journal of Biomechanics 40 (2007) 3363–3372

JOURNAL OF BIOMECHANICS

www.elsevier.com/locate/jbiomech
www.JBiomech.com

Three-dimensional finite element modelling of muscle forces during mastication

Oliver Röhrle[a,*], Andrew J. Pullan[a,b]

[a]*Bioengineering Institute, The University of Auckland, Private Bag 92019, Auckland 1, New Zealand*
[b]*The Department of Engineering Science, Faculty of Engineering, The University of Auckland, Private Bag 92019, Auckland 1, New Zealand*

Accepted 5 May 2007

Abstract

This paper presents a three-dimensional finite element model of human mastication. Specifically, an anatomically realistic model of the masseter muscles and associated bones is used to investigate the dynamics of chewing. A motion capture system is used to track the jaw motion of a subject chewing standard foods. The three-dimensional nonlinear deformation of the masseter muscles are calculated via the finite element method, using the jaw motion data as boundary conditions. Motion-driven muscle activation patterns and a transversely isotropic material law, defined in a muscle-fibre coordinate system, are used in the calculations. Time–force relationships are presented and analysed with respect to different tasks during mastication, e.g. opening, closing, and biting, and are also compared to a more traditional one-dimensional model. The results strongly suggest that, due to the complex arrangement of muscle force directions, modelling skeletal muscles as conventional one-dimensional lines of action might introduce a significant source of error.

Keywords: Finite element method; Skeletal muscle modelling; Finite elasticity; Human mastication

1. Introduction

Mastication of solid food is a complex process in which the size of the food particles is reduced and saliva is incorporated to form a bolus suitable for swallowing. In this process, the muscles of mastication are predominantly responsible for controlling the position of the mandible (lower jaw) and generating the appropriate amount of force. A chewing cycle is controlled, as is all skeletal locomotion, by neural circuitry called central pattern generators (Lund, 1991). The physiological complexity of this chewing system and the fact that the muscle forces cannot be measured experimentally make mathematical models of the muscles of mastication indispensable for analysing human chewing.

One common characteristic of virtually all studies aimed at investigating different aspects of the human masticatory system is the fact that the muscles of mastication, or a particular subgroup of them, are represented as one-dimensional elastic strings. For example, Koolstra et al. use such a representation to analyse unloaded jaw-opening and jaw-closing movements in humans (Koolstra, 1997a, b, Koolstra and van Eijden, 2001) as well as to examine maximal biting forces (Koolstra et al., 1988). Others have used a linear representation of the muscle's line of action to investigate patterns of bone remodelling (Ichim et al., 2006), to estimate temporomandibular joint reaction forces (May et al., 2001), to predict tensions, deformations (Koolstra and van Eijden, 2005), and volumetric strain of the temporomandibular joint cartilage (Koolstra and van Eijden, 2006), and to assess loading conditions of a temporomandibular joint prosthesis (van Loon et al., 1998). Even anthropologists have adopted these models to debate the anatomical basis for the Neandertal's unique craniofacial morphology and the evolutionary mechanism that produced this unique morphology (O'Connor et al., 2005).

To represent the behaviour of a full three-dimensional muscle by one-dimensional strings simplified physiological information is needed. In the above mentioned works, the

*Corresponding author. Tel.: +64 9 373 7599x85353; fax: +64 9 367 7157.
E-mail address: o.rohrle@auckland.ac.nz (O. Röhrle).

0021-9290/$ - see front matter © 2007 Elsevier Ltd. All rights reserved.
doi:10.1016/j.jbiomech.2007.05.011

average muscle length, the point of origin, the direction, and the resulting attachment points were used. These were obtained either by examining multiple cadavers (van Eijden et al., 1997) or by means of determining the centreline of three-dimensional representations obtained from MRI scans (Koolstra et al., 1990; Cattaneo et al., 2005).

For one-dimensional skeletal muscle models, multiple approaches are used to calculate the forces but all of them are based on the physiological cross-sectional area (PCSA). Weijs and Hillen (1985) assume proportionality of the PCSA and the muscle force. Barbenel (1974) combines the PCSA with experimentally obtained electromyographic (EMG) data to calculate estimates for instantaneous muscle forces. Koolstra and van Eijden (2001) include active and passive elements by describing the muscles of mastication with Hill-type flexible, single-line actuators.

One of the major unknowns in modelling skeletal muscles as one-dimensional strings is how well these represent the behaviour of the full three-dimensional muscle. Throckmorton (1985) and Koolstra et al. (1988) suggested that the force direction may have significant influence on the mechanical performance of the masticatory system. In particular, Koolstra et al. (1988) stated that the direction of the masseter's lines of action has a significant influence on possible maximum bite forces. Furthermore, it is clear that reducing the complexity of muscles to strings neglects entirely the variation of muscle density and structure. The development of a validated three-dimensional model framework for the muscles of mastication would allow one to include a more detailed description of their anatomical and physiological characteristics, as well as providing a mechanism by which those using one-dimensional modelling could quantify such an approximation.

To our knowledge, mathematical models representing muscles as three-dimensional objects do not exist in the field of mastication, although there have been a few instances of the use of such three-dimensional models in the analysis of other skeletal muscles. Blemker et al. (2005) developed a three-dimensional finite element model for the biceps brachii, as well as for the rectus femoris and vastus intermedius, while Oomens et al. (2003) developed three-dimensional models for the tibialis anterior of the rat, and Lemos et al. (2005) for the human tibialis anterior.

The purpose of this paper is to introduce a three-dimensional finite element model to calculate and investigate directions and magnitudes of muscle forces generated by the left and right masseter muscle during one chewing cycle. In what follows, we present the methods used to create and solve the model, and then present the key results of the computations. We end with the discussion of the results and address the limitations of this study.

2. Methods

Given a three-dimensional geometrical model of the human masticatory system (Fig. 1), the proposed method of calculating directions and magnitudes of muscle forces generated by the left and right masseter muscles can be summarised as:

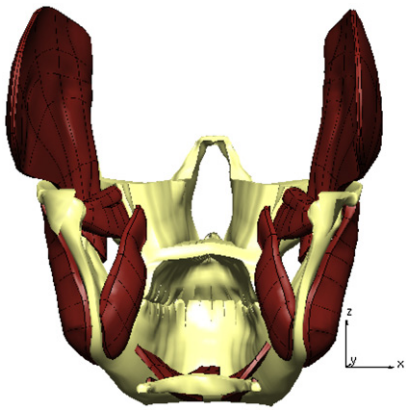

Fig. 1. Geometry (and orientation of the coordinate system) of the muscle of mastication and bone (viewed from the back to highlight all muscles) as presented in van Essen et al. (2005). The black lines on top of the muscle geometries (red) represent the element boundaries of the cubic Hermite finite element discretisation used for the numerical simulations. The model of the muscles of mastication was constructed from the Visible Man project Spitzer et al., 1996 and augmented with data from various anatomical and physiological texts.

Step 1: Collecting a six degree of freedom kinematical data set describing natural chewing.

Step 2: Extending our existing mathematical models of the masseter muscles to include muscle fibre distributions within the muscles.

Step 3: Defining a constitutive law in the muscle fibre coordinate system that is capable of capturing components of active and passive muscle behaviour.

Step 4: Solving the continuum-based equations of finite elasticity using the above model, constitutive law, and boundary conditions.

2.1. Step 1: Collection of the chewing data

The first challenge in modelling masseter muscle deformation during mastication is imposing a natural mandibular movement on the model. This is an essential step as this movement prescribes the displacement boundary conditions for the muscle attachment areas needed in Step 4.

An opto-electronic motion capturing system, a Vicon MX,[1] was used to record chewing data in three dimensions with six degrees of freedom (Röhrle et al., 2007). The locations of three markers (with respect to one overall coordinate system) attached to the head (on a tight-fitting swimming cap) and of three fixed markers rigidly attached to a custom-made appliance were used to track the movement of the mandible at a frequency of 100 Hz while chewing standardised food (Foster et al., 2006; 0.0891 ± 0.003 MPa maximum stress at 50% compression). The quality of the recordings was quantified by looking at the standard deviation of the recorded Euclidean distance between two markers on the appliance. The calculated standard deviation was less than 0.07 mm (Röhrle et al., 2007).

The coordinates of all six marker locations are used to describe the dynamics of the mandible. While the three head markers are used to remove any head movement, the movement of the markers on the appliance (after being corrected by the respective head movement) are used to describe the mandibular movement within the model. For this purpose, the mandible is assumed to be rigid. For each recorded time step, there exists a rigid-body transformation that maps the three marker locations on the appliance of the first time step to the marker's location at the current time step. (The exact method to find the rigid body transformation under the presence of small recording errors is explained

[1]The Biomechanics Laboratory, Department of Sports and Exercise Science, University of Auckland, Tamaki Campus.

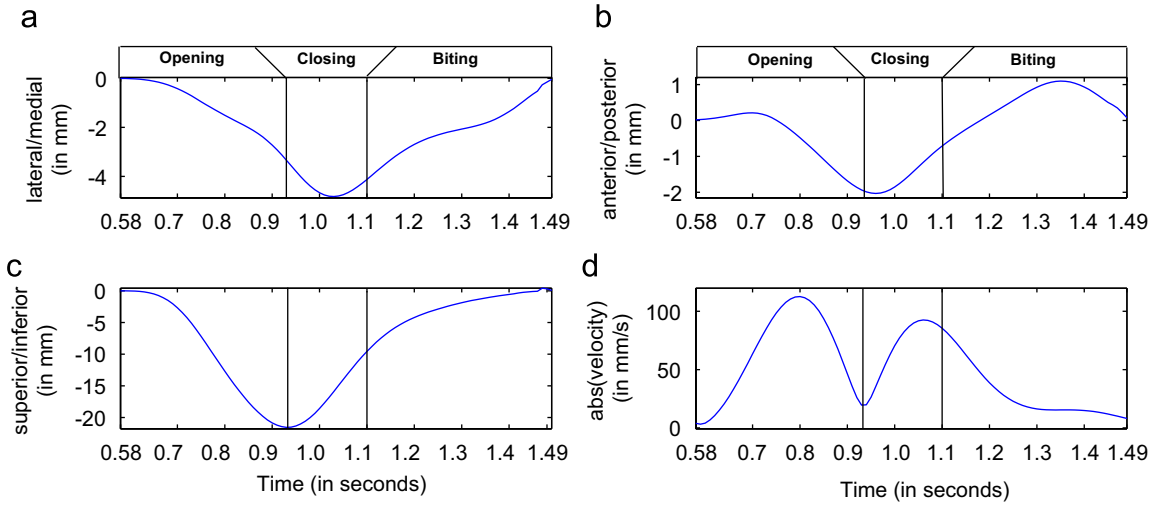

Fig. 2. Three-dimensional chewing trajectory of the first chewing cycle at the interincisal position: Displacements (a)–(c) and velocity (d) versus time.

in detail in Röhrle et al., 2007.) Note that starting the recordings in a closed mouth position naturally links the initial recording position with the model reference position. The measured kinematics are imposed upon the model by applying the respective rotations and translations for each time step and every node point on the mandible.

Fig. 2 displays the displacement (Fig. 2 (a)–(c)) and velocity (Fig. 2 (D)) for one chewing cycle (0.58–1.49 s) at a nodal point on the model located at the cusps in between the front incisors of the mandible (the interincisal position). As there was minimal movement during the first chewing cycle for $t<0.58$ s , the data were excluded from the plots.

As indicated in Fig. 2, the chewing cycle is divided into an opening, closing, and biting phase. The opening phase lasts until the distance between the upper and lower incisors starts to decrease. The beginning of the biting phase is determined by the distance between the upper and lower first premolar. The subject is considered to be biting if that distance is less than 10 mm, the height of the model food used during the recordings. Hence, based on the recordings presented in Fig. 2, the mandible is in the opening phase for $t<0.93$ s, the closing phase for $0.93\,\text{s}\leqslant t<1.11$ s, and the biting phase for $1.11\,\text{s}\leqslant t<1.50$ s.

2.2. Step 2: The fibre field

All simulations within this paper were carried out with the software package CMISS,[2] which has been used extensively for continuum modelling of the heart (Nash and Hunter, 2000; Hunter et al., 2003), the lungs (Tawhai et al., 2004), and the digestive system (Pullan et al., 2004). The three-dimensional FEM implementation of finite elasticity within CMISS is described in detail by Nash and Hunter (2000). The method's key characteristic is that it uses, for the reference state, a locally varying material coordinate system, v_α, in addition to a global coordinate system. The locally varying coordinate system is typically aligned with structural features. In the heart these features are the muscle fibre direction (f), the muscle sheet direction (s), and the sheet-normal direction (n).

Within this framework all spatially varying quantities are hence expressed with respect to the material coordinate system, e.g. the Green strain tensor, $[E_{\alpha\beta}]$, or the second Piola–Kirchhoff stress tensor, $[T^{\alpha\beta}]$ where $\alpha,\beta=f,s,n$. Stress equilibrium can then be derived from the principle of virtual work, and is given, in terms of the v_α-coordinate system, by the following equation:

$$\int_{V_e} T^{\alpha\beta}F^j_\beta\delta u_{j,\alpha}\,\mathrm{d}V_e=\int_{V_e}\rho_0(b^j-f^j)\delta u_j\,\mathrm{d}V_e+\int_{S_e}s^j\delta u_j\,\mathrm{d}S_e. \tag{1}$$

Here F^j_β are the components of the deformation gradient with respect to the v_α-coordinate system, $\delta u_{j,\alpha}$ are the virtual displacements expressed relative to the reference coordinate system and differentiated with respect to the v_α-coordinate system, ρ_0 is the material density in the reference configuration, b_j and f_j are the body force and acceleration vector, and s^j is the loaded surface traction on the surface, S_e, of volume V_e.

To apply the above material coordinate system methodology to skeletal muscles, it is essential to identify the appropriate structural features of skeletal muscles. Skeletal muscles are made up of long fibres and the muscles are therefore rather elongated and of cylindrical shape. They exhibit different material properties in the fibre direction and the transverse plane. Hence, in our skeletal muscle model the f-direction is aligned with the skeletal muscle fibre direction, whereas the s- and n-directions are chosen in such a way that they span a plane orthogonal to the f-direction (i.e. transversely isotropic).

The masseter muscle consists of a superficial and a deep portion. The larger superficial portion arises from the zygomatic bone and its fibres pass downward and backward to be inserted into the lower half of the lateral surface of the ramus of the mandible. The deep portion of the masseter is much smaller and more muscular in texture. It arises from posterior parts of the zygomatic arch. Its fibres pass downward and forward and are inserted into the upper half of the ramus. The deep portion of the muscle is partly concealed by the superficial portion.

Although it would be desirable to base the model fibre geometry on measurements of actual muscle fibres, it was not possible to find applicable data for this. Instead, an approach similar to the one proposed by Blemker and Delp (2005) is used to obtain an anatomical-based approximation of the complex fibre geometry. For this purpose, the existence of tendons within the masseter are ignored and the deep and superficial muscles are treated as one entity. Furthermore, it is assumed that the muscle fibres (fascicles) are attached directly to the mandible and maxilla. Then, similar to Blemker and Delp (2005), rational Bezier spline curves are used to describe a particular fibre field within a template geometry. In our case, the template for the masseter muscle consists of two stacks each with 7 unit cubes (see Fig. 3). These numbers are chosen in such a way that the template matches the number of elements of the finite element discretisation for the masseter muscle (1 element wide in the x-direction, 2 elements wide in the y-direction, and 7 elements in the z-direction). A one-to-one mapping is then used to derive the fibre structure within the actual masseter geometry.

[2]An interactive computer program for Continuum Mechanics, Image analysis, Signal Processing and System Identification developed at the Bioengineering Institute at the University of Auckland (http://www.cmiss.org/).

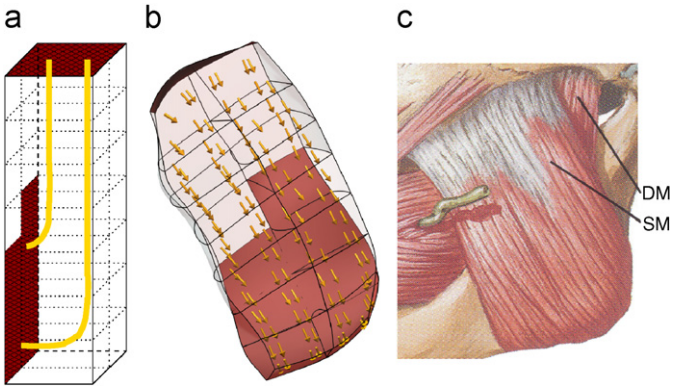

Fig. 3. Directions of the fibre field in (a) the template, (b) within the final geometry, and (c) schematic drawing of the deep (DM) and superficial masseter (SM) (from Netter, 2003). In (a) and (b), the attachment areas of the muscle to the mandible (on the left) and maxilla (on the top) are shown in red.

To express spatially varying quantities with respect to the fibre orientation within the finite element simulations, it is necessary to define a field within each element that describes the global fibre field orientation and can be approximated by basis functions associated with parameters defined at the element nodes (see Nielsen et al., 1991). The fibre field is obtained by mapping the template fibre distribution at a total of 7220 equally spaced points to the geometry of the masseter and then using cubic Hermite basis functions to fit the fibre field. The result of this fitting process is depicted in Fig. 3(b). The fibre directions are indicated by (golden) arrows. The advantage of such a fitted fibre field is that one can now easily define at any location a local material coordinate system v_α.

Note that the template fibre distribution is only necessary because no actual data on the fibre geometry was available. If such data were available, one would, of course, use this information to describe at sufficiently many grid points the respective fibre directions. This has been done, for instance, in the heart (Nielsen et al., 1991).

2.3. Step 3: Definition of the Constitutive Law

The constitutive law for the transversely isotropic material used within this paper is obtained by adding additional stress components to an isotropic material law. These additional components stem from passive and active responses along the fibre direction in order to increase the stiffness of the material in that particular direction. This approach is similar to the one proposed in Lemos et al. (2005), Blemker et al. (2005) and Blemker and Delp (2006).

Skeletal muscle can be described as a hyperelastic, incompressible, and transversely isotropic material. For such materials, constitutive laws can be derived mathematically by postulating a strain energy function, $\mathbf{W}$, which can be seen as a scalar potential that depends on the components of either the Green's strain tensor, $\mathbf{E}$, the Cauchy–Green deformation tensor, $\mathbf{C}$, or its invariants (see, Criscione et al., 2001). The isotropic invariants $I_1 - I_3$ are used to describe the strain energy function part for the underlying isotropic material (a Mooney–Rivlin material) with I_3 being the invariant associated with the volume change. Invariant I_4 is the square of the fibre stretch, λ, while I_5 is entirely ignored within this formulation. The strain energy function for a Mooney–Rivlin material is given by

$$\mathbf{W}(I_1, I_2, I_3) = \overline{\mathbf{W}}(I_1, I_2) + \kappa(I_3 - 1), \tag{2}$$

with

$$\overline{\mathbf{W}}(I_1, I_2) = c_1(I_1 - 3) + c_2(I_2 - 3), \tag{3}$$

where κ is a scalar that, under certain circumstances, can be associated with the hydrostatic pressure, p. The strain energy function, $\mathbf{W}$, can be decomposed into a deviatoric and a hydrostatic part. Thus, $\mathbf{W}$ can be expressed in terms of the distortional component of the right Cauchy–Green tensor $\tilde{\mathbf{C}} = J^{-2/3}\mathbf{C}$, where J is the determinant of the deformation gradient tensor, $\mathbf{F}$, or its respective invariants $\tilde{I}_1$ to $\tilde{I}_4$. With $\kappa = -\frac{1}{2}p$, one then obtains the components of the stress tensor with respect to material coordinates by differentiating (2) with respect to the strain tensor components, $E_{\alpha\beta}$. Hence,

$$T^{\alpha\beta}_{\text{iso}} = \frac{\overline{\mathbf{W}}(\tilde{I}_1, \tilde{I}_2)}{\partial E_{\alpha\beta}} - p\delta^{\alpha\beta}, \tag{4}$$

where $\alpha, \beta = f, s, n$ and $\delta^{\alpha\beta}$ is the Kronecker delta.

Next, it is assumed that the passive resistance grows with respect to the fibre stretch, λ, but only in the fibre direction, f, of the skeletal muscle. Therefore only one term of the true (Cauchy) stress tensor is altered and the full Piola–Kirchhoff stress tensor with respect to the micro-structural axes can be written as

$$T^{\alpha\beta}_{\text{passive}} = T^{\alpha\beta}_{\text{iso}} + J(\sigma^{ff}_{\text{passive}} f^{\text{fibre}}_{\text{passive}}(\lambda))\frac{\partial X^\alpha}{\partial v_f}\frac{\partial X^\beta}{\partial v_f}, \tag{5}$$

where $f^{\text{fibre}}_{\text{passive}}(\lambda)$ is a normalised force curve depending on the fibre stretch and $\sigma^{ff}_{\text{passive}}$ is a constant Cauchy stress such that the product equals the additional stress induced from stretching the object in the f-direction, and $\frac{\partial X^\alpha}{\partial v_f}$ the inverse of the deformation tensor with respect to f-component of the v_α-coordinate system. The function $f^{\text{fibre}}_{\text{passive}}(\lambda)$ is defined by

$$f^{\text{fibre}}_{\text{passive}}(\lambda) = \begin{cases} 0, & \lambda \leqslant 1, \\ P_1(e^{P_2(\lambda-1)} - 1)), & 1 < \lambda \leqslant \lambda_{\text{ofl}}, \\ P_3\lambda + P_4, & \lambda > \lambda_{\text{ofl}}, \end{cases} \tag{6}$$

and is depicted in Fig. 4 by the (blue) dashed line. The constants P_1 to P_4, and the optimal fibre stretch length, λ_{ofl}, used within this paper are listed in Table 1.

In order to take into account the effect of muscle fibre length an active component is added to $T^{\alpha\beta}_{\text{passive}}$. To control the level of activation, a parameter α is introduced that can be interpreted as the percentage of

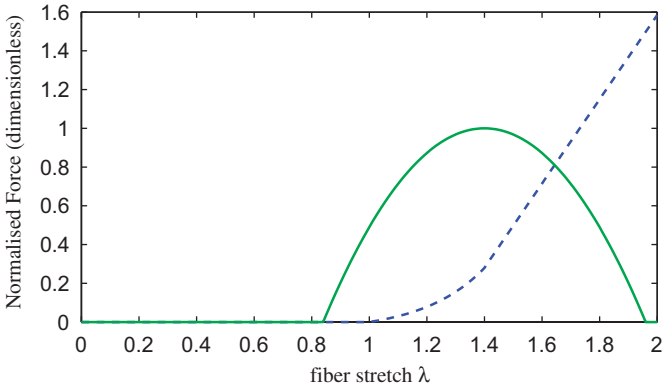

Fig. 4. Normalised force versus fibre stretch relationships for $f^{\text{fibre}}_{\text{passive}}(\lambda)$ (dashed line) and $f^{\text{fibre}}_{\text{active}}(\lambda)$ (solid line).

Table 1
Actual values used for constants in $f^{\text{fibre}}_{\text{passive}}(\lambda)$ and $f^{\text{fibre}}_{\text{active}}(\lambda)$

Constant	Value	Constant	Value
c_1	0.01 MPa	c_2	0.01 MPa
P_1	0.05	P_2	6.6
P_3	2.1751	P_4	−2.7655
$\sigma^{ff}_{\text{passive}}$	0.3 MPa	$\sigma^{ff}_{\text{active}}$	0.3 MPa
λ_{ofl}	1.4		

active muscle fibres. Hence,

$$T^{\alpha\beta}_{\text{active}} = T^{\alpha\beta}_{\text{passive}} + J\left(\alpha\sigma^{ff}_{\text{active}} f^{\text{fibre}}_{\text{active}}(\lambda)\right)\frac{\partial X^{\alpha}}{\partial v_f}\frac{\partial X^{\beta}}{\partial v_f}, \tag{7}$$

where $\alpha \in [0, 1]$ and

$$f^{\text{fibre}}_{\text{active}}(\lambda) = \begin{cases} -\frac{25}{4\lambda^2_{\text{ofl}}}\lambda^2 + \frac{25}{2\lambda_{\text{ofl}}}\lambda - 5.25 & 0.6\lambda_{\text{ofl}} \leqslant \lambda \leqslant 1.4\lambda_{\text{ofl}}, \\ 0 & \text{otherwise.} \end{cases} \tag{8}$$

The function was chosen such that $f^{\text{fibre}}_{\text{active}}(\lambda)$ is quadratic, equals 1 at the optimal fibre length stretch λ_{ofl}, and 0 for fibre stretch values smaller than $0.6\lambda_{\text{ofl}}$ or greater than $1.4\lambda_{\text{ofl}}$. The function is depicted in Fig. 4 by the solid (green) line.

Table 1 and Fig. 4 define all parameters except for the activation parameter, α. Since the masseter muscles are mainly active during closing, it is assumed that the masseter muscles exhibit very little activity during the opening phase ($0\,\text{s} < 0.93\,\text{s}$). Therefore, the value α is linearly increased from 0 to 0.05 over the entire opening phase. Once the mandible starts closing, at $t = 0.93\,\text{s}$, the level of activation is increased to $\alpha = 0.3$ after 0.05 s. The biting phase is modelled by a constant activation level of $\alpha = 0.9$, which is achieved by linearly increasing α over 0.05 s to 0.9 at $t = 1.11\,\text{s}$, and decreasing it to 0 at its end. The same activation pattern is used throughout the left and right masseter and does not vary with location (see Fig. 7).

2.4. Step 4: Solving the continuum-based equations of finite elasticity

At each time step, a Galerkin finite element method with cubic Hermite basis functions is used to discretise the weak formulation (Eq. (1)) of the

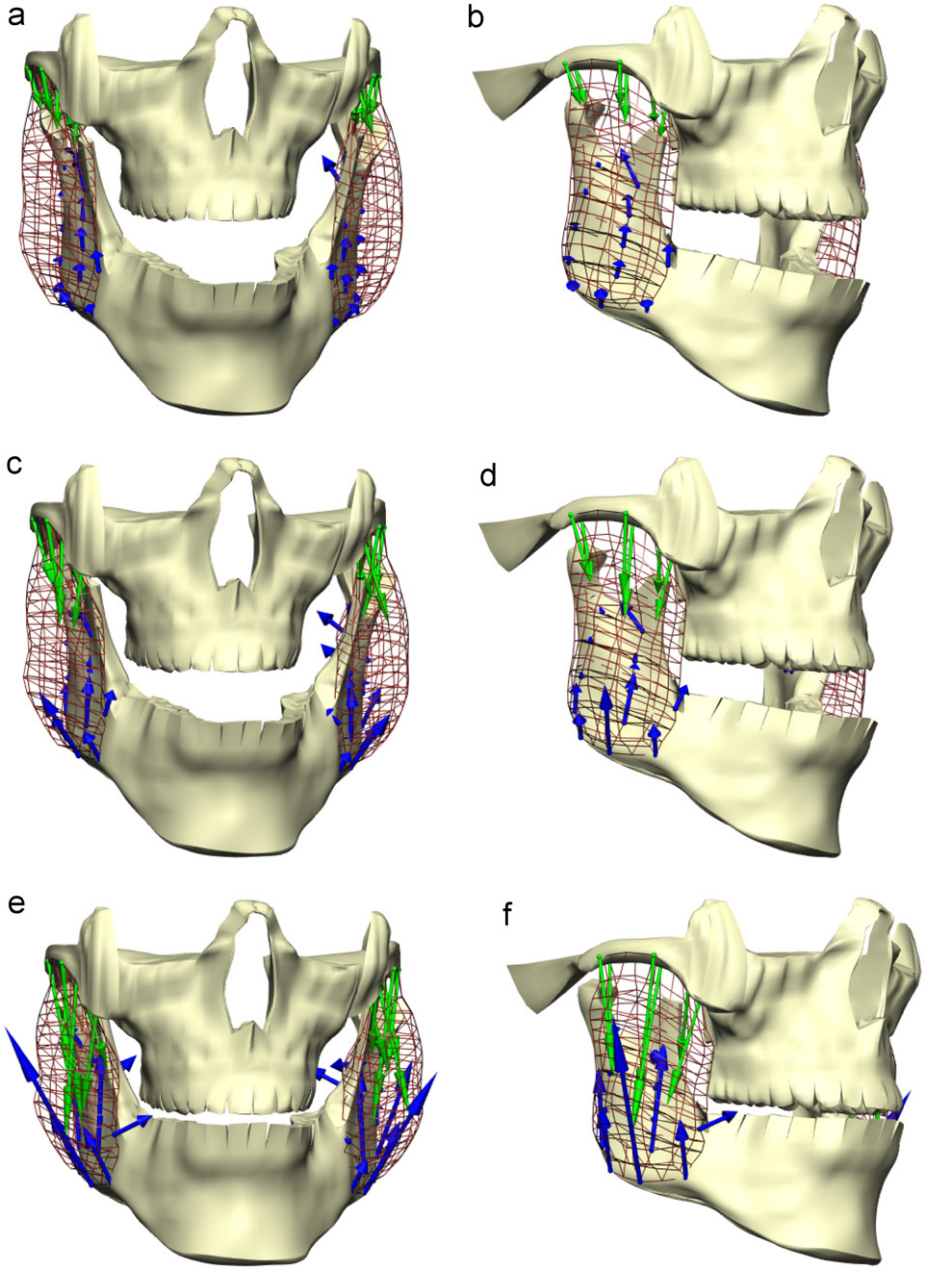

Fig. 5. Front and side views of the mandible, maxilla, and right and left masseter muscles at $t = 0.93\,\text{s}$, $t = 1.00\,\text{s}$, and $t = 1.23\,\text{s}$ during the simulation of the chewing cycle depicted in Fig. 2. The green arrows at the maxilla and the blue arrows at the mandible depict the direction of the muscle forces generated at the attachment area. Their lengths are scaled by the magnitude of the calculated muscle force.

continuum-based equations of finite elasticity. Boundary conditions are specified at the nodal values in the region of the muscle attachment areas at the mandible and maxilla. At the maxilla, all nodal values are fixed. At the mandible, the displacement boundary conditions are calculated as the difference between the reference state (closed mouth position) and its respective values calculated by the rigid body movements for the current mandibular position.

3. Results

The magnitudes and directions of the muscle forces acting on the mandible and maxilla are extracted from the FEM simulations (Fig.5) in order to establish time–force relationships (Fig. 6) and to compare its directions with a one-dimensional model (Fig. 8).

Fig. 5 reveals the complexity of the muscle forces acting on the mandible and maxilla. In particular, it depicts the spatial and task-dependent variations of muscle forces. The local lines of action, defined by the directions of the computed force vectors at the attachment areas of mandible and maxilla, are depicted as green arrows at the maxilla and as blue ones at the mandible. The length of the arrows is scaled by the magnitude of the muscle force. The results in Fig. 5 demonstrate that the distribution of the force vectors not only varies with respect to its location, but also with respect to time and task. For example, the positions of the maximal force vary according to the different phases of the chewing cycle. During opening, the force is maximal at a point towards the middle and superior regions of the mandibular attachment area, whilst during biting the maximal force is towards the inferior region of the attachment area.

In order to quantitatively present and analyse such complex muscle force distributions, it is reasonable to define, for each side and attachment area, one representative force vector, $\mathbf{F}^{i,j} = (F_x^{i,j}, F_y^{i,j}, F_z^{i,j})$, where $i \in \{\text{Mandible, Maxilla}\}$ and $j \in \{\text{left, right}\}$. This is done by adding up, for each of the four attachment areas, the respective forces calculated at each of the four attachment areas. For example, $\mathbf{F}^{\text{Maxilla,right}}$, is the sum of the six (green) force vectors, which originate in Fig. 5 from the right maxilla. The components of the calculated force vectors, $F_x^{i,j}, F_y^{i,j}$, and $F_z^{i,j}$, as well as the magnitude of the overall forces, $\|\mathbf{F}^{\text{Mandible},j}\|$ and $-\|\mathbf{F}^{\text{Maxilla},j}\|$ are depicted in Fig. 6. The minus sign in front of $\|\mathbf{F}^{\text{Maxilla},j}\|$ is simply to take into account the general force direction at the maxilla.

The maximum computed forces of 76.98 N (right masseter) and 67.9 N (left masseter) are obtained at $t = 1.18$ s during biting. Before actual biting occurs, the maximum calculated forces are obtained at $t = 0.99$ s and they are 43.85 N for the right masseter and 43.02 N for the left masseter. In the opening phase, the force steadily increases until it reaches its maximum at the end of the opening phase ($t = 0.93$ s) with computed values 23.07 N (right) and 23.75 N (left).

Fig. 7 depicts the values of the two most important constitutive law parameters, the fibre stretch, λ, and the profile for the activation parameter, α, as functions of time. The values for λ in Fig. 7 correspond to the average fibre stretch values, λ^{avg}, which is defined as the geometric average of the fibre stretch values at all points of the respective attachment areas. At the masseter, λ^{avg} is larger during biting ($1.1 < \lambda^{\text{avg}} < 1.27$ (left) and 1.2 (right)) than during the opening or closing phase ($\lambda^{\text{avg}} < 1.13$). At the maxilla, λ^{avg} is overall much larger, with maximal values of 2.34 (right) and 2.28 (left) during biting, 2.23 (right) and 2.13 (left) during closing, and less than 1.82 (right) and 1.75 (left) during the opening phase.

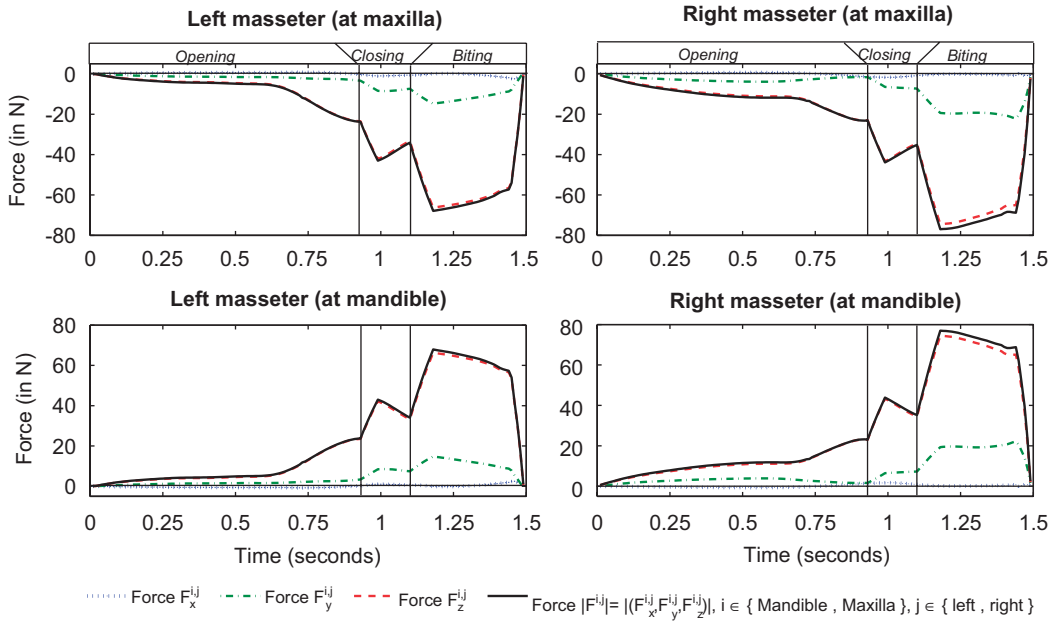

Fig. 6. Calculated forces at the maxilla (left and right) and mandible (left and right) during one chewing cycle.

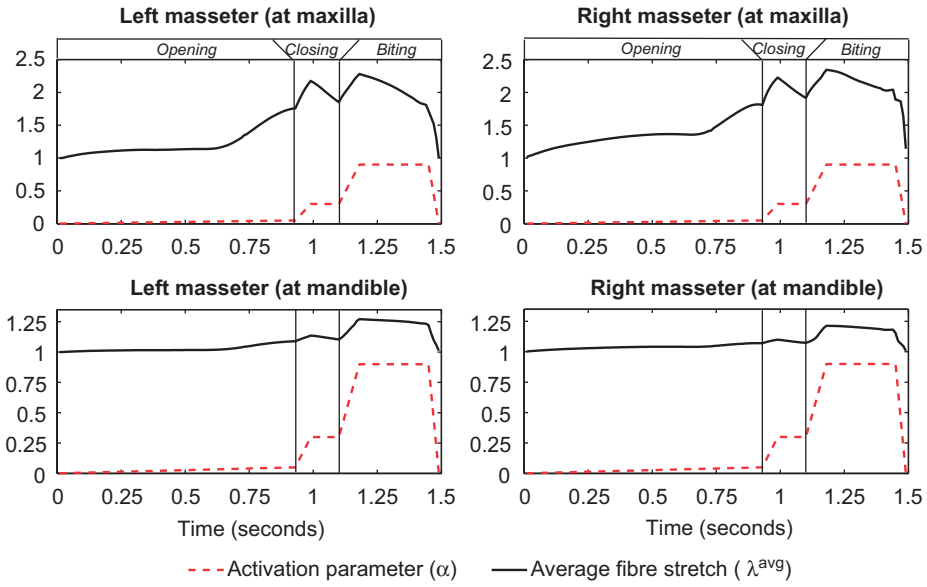

Fig. 7. Activation level α and computed averaged fibre stretch, λ^{avg}, during one chewing cycle at the right and left side of the mandible and maxilla.

While an extensive analysis between one- and three-dimensional models is beyond the scope of this paper, it is still worthwhile to include some quantitative comparisons, e.g. a comparison between the direction of the force $\mathbf{F}^{\text{Mandible,right}}$ and the respective one-dimensional line of action, which is defined as the force direction obtained from a one-dimensional model of the right masseter. In this paper, the line of action is computed from the Visible Man data set using an iterative algorithm similar to the one proposed in Koolstra et al., 1989. (Here, the iterative process was stopped after consecutive approximations of the line of action differed by less than 0.3°.) To take into account the chewing kinematics, the same motion used in the three-dimensional model is imposed on the mandibular attachment point of the reconstructed one-dimensional line of action. Then, for each time step, the normalised direction of the line of action, d_{1D}, is compared to the normalised force $\mathbf{F}^{\text{Mandible,right}}$, d_{3D}, by computing the angle between these directions. The angle Φ, is computed using the inner product, i.e. $\Phi := \cos^{-1}(\langle d_{1D}, d_{3D} \rangle)$. The results are depicted in Fig. 8.

From Fig. 8, it appears that the directions of the line of action and the force $\mathbf{F}^{\text{Mandible,right}}$ are more strongly dependent on the position of the mandible (open/closed) than with the activation level of the masseter. For example, the deviation between the line of action and $\mathbf{F}^{\text{Mandible,right}}$ remains below 3.5° for an interval of 0.16 s before and 0.12 s after maximum opening ($t = 0.93$ s). The smallest deviation (0.68°) is obtained at $t = 0.97$ s. In contrast, for most parts of the biting phase and at the beginning of the opening phase, when the teeth are still close to contact, the angle between the two directions varies between 10° and 16°.

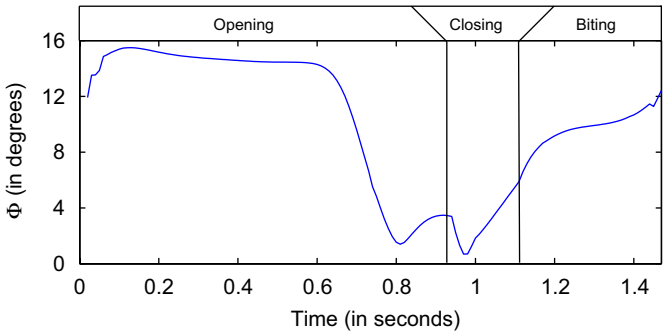

Fig. 8. Angle Φ between the directions of the line of action from a one-dimensional model and the force, $\mathbf{F}^{\text{Mandible,right}}$, obtained from the three-dimensional model.

4. Discussion

The main objective of this work is to introduce a three-dimensional finite element model to calculate and investigate the directions and magnitudes of muscle forces generated by the left and right masseter muscle during one chewing cycle. The central results for this work are given in Fig. 5. These results illustrate the highly complex masseter muscle force distributions during a single chewing cycle. The muscle force distributions depicted in Fig. 5 and the comparison of the resulting force vectors from one- and three-dimensional models (Fig. 8) demonstrate one of the outcomes that differ between these two models.

Fig. 8 shows the deviations between one- and three-dimensional models are still present even after reducing the locally varying muscle forces to one force vector per attachment area. According to Fig. 8, the deviations are

most substantial in near closed-mouth position (between 10° and 16°). Furthermore, this range seems to be quite independent of muscle activity. The deviations appear to be large enough to influence some of the outcomes of studies, which base their model on a (near) closed-mouth position and on one-dimensional representations of the masseter, e.g. studies investigating maximal bite forces or clenching. However, without repeating the numerical experiments of previous studies, it can only be speculated as to how much such deviations affect these results. In this context, it is also essential to perform a sensitivity analysis on the constitutive parameters and the fibre field distribution to investigate their effects on the deviation of muscle forces derived from one- or three-dimensional models.

As with all such studies, the work presented here has a number of limitations. First, the data used to construct the anatomical model and those used to obtain the kinematic chewing data were obtained from different individuals. It is well known that the craniofacial anatomy of the bony structures, for example the anatomy of the temporomandibular joint, can vary significantly from person to person. To avoid (modelling) collisions between the mandible and the skull, the geometry of the model and the kinematic data should ideally stem from the same subject. Although the FEM model was derived from the Visible Man (Spitzer et al., 1996) and a different subject was used for recording the chewing data, no collisions were noted.

Another limitation of the modelling work is the fact that the computed muscle forces are at the lower end of published values. The maximum value reported in this study is about 77 N whereas published force values have exceeded >200 N (Koolstra and van Eijden, 2005 or Korioth et al., 1992). The choice of material parameters used within the constitutive law (Table 1) and the fact that the model simulates chewing and not maximal biting might explain the discrepancy. Numerical experiments showed that whilst reasonable deviations of the key constitutive parameters ($c_1, c_2, \sigma^{ff}_{\text{passive}}, \sigma^{ff}_{\text{active}}$) do affect the magnitude of the generated force, they do not affect the direction of the muscle forces (Fig. 5) or the overall shape of the time–force curve greatly (Fig. 6). This in turn suggests that the fibre distribution plays the most important role in accurately determining the directions of the muscle forces acting on the mandible or skull. If so, an accurate anatomical representation of the internal muscle fibre structure might give the next significant advancement in understanding muscle forces generated by the masseter, or skeletal muscles in general.

The activation parameter, α, plays a key role in this study. The values, $\alpha = 0.3$ and $\alpha = 0.9$, were chosen to properly distinguish between closing and biting. Note that a change of $\sigma^{ff}_{\text{passive}}$ and $\sigma^{ff}_{\text{active}}$ redefines its proportional relationship. It is of fundamental importance to derive accurate constitutive parameters from experimental data such that α can be directly linked, and not just interpreted, to a physiological quantity. Then, EMG measurements could play an important role in determining task-specific values for α. However, the authors believe that the given model should still be good enough to further investigate task-related differences of muscle forces and their distributions based on, for example, data of spatially varying activation patterns as investigated by McMillan and Hannam (1992).

The three-dimensional model of the masseter muscle proposed in this paper should be seen as an extendable framework to gain a better understanding of muscle mechanics and to advance skeletal muscle models in general. The model still needs to address deficiencies in the description of the constitutive behaviour as well as deficiencies in its description of the anatomically complex muscle architecture, in particular, the inclusion of tendons. In that regard, the software package CMISS is an extremely powerful tool. It has been designed to augment the continuum-based equations of finite elasticity to include micro-structural details and to incorporate a variety of constitutive laws that bridge spatial scales from cellular levels to the whole organs (Hunter and Borg, 2003). The full potential and advantages of such powerful tools, however, cannot be fully exploited as long as (parts of) models cannot be validated or fitted to experimental data. While there has been extensive research focusing on developing frameworks to describe constitutive laws based on experimental data for the myocardium (Sacks and Sun, 2003; Hunter et al., 2003; Humphrey, 2002), there exist, to the authors' knowledge, no similar studies for skeletal muscles. Hence, the constitutive law described in Section 2.3 focuses, like the ones used in Blemker et al. (2005), Oomens et al. (2003), and Lemos et al. (2005), on capturing the key characteristics of skeletal muscle. In future research, it is essential to develop constitutive descriptions which match experimental data.

The list of advantages of three-dimensional models over one-dimensional models is long. Another important advantage, not mentioned much within this study, is the fact that three-dimensional models dynamically simulate shape changes of the muscle. This, for example, plays an important role if one is interested in investigating changes of biomechanical muscle properties, which depend on extramuscular force transmission induced, for example, by the surrounding muscle tissue, fat, or skin (Yucesoy et al., 2003; Teran et al., 2005). Furthermore, comparisons between (regional) strain calculations and image-based two-dimensional estimates derived from new displacement encoding methods based on MRI (DENSE, Aletras et al., 1999; Kim et al., 2004) could deliver new and promising ways of estimating or validating constitutive parameters. Moreover, the comparison of stresses and strains in generic and "healthy" models with pathological cases might aid in identifying treatment methods for musculoskeletal-induced diseases.

In summary, despite the limitations outlined above, there is good evidence to suggest that the muscles force distributions are highly complex and do not readily lend themselves to simple one-dimensional representations.

Conflict of interest

The authors declare that there is no conflict of interest present.

Acknowledgement

This work was funded through the Foundation for Research in Science and Technology (FRST) under contract number UOAX0406.

References

Aletras, A., Ding, S., Balaban, R., Wen, H., 1999. Dense: displacement encoding with stimulated echoes in cardiac functional mri. Journal of Magnetic Resonance 137, 247–252.

Barbenel, J., 1974. The mechanics of the temporomandibular joint—theoretical and electromyographical study. Journal of Oral Rehabilitation 1 (1), 19–27.

Blemker, S., Delp, S., 2005. Three-dimensional representation of complex muscle architectures and geometries. Annals of Biomedical Engineering 33 (5), 661–673.

Blemker, S.S., Delp, S.L., 2006. Rectus femoris and vastus intermedius fiber excursions predicted by three-dimensional muscle models. Journal of Biomechanics 39, 1383–1391.

Blemker, S., Pinsky, P., Delp, S., 2005. A 3d model of muscle reveals the causes of nonuniform strains in the biceps brachii. Journal of Biomechanics 38 (4), 657–665.

Cattaneo, P., Kofod, T., Dalstra, M., Melsen, B., 2005. Using the finite element method to model the biomechanics of the asymmetric mandible before, during and after skeletal correction by distraction osteogenesis. Computer Methods in Biomechanics and Biomedical Engineering 8 (3), 157–165.

Criscione, J., Douglas, A., Hunter, W., 2001. Physically based strain variant set for materials exhibiting transversely isotropic behavior. Journal of Mechanics and Physics of Solids 49, 871–897.

Foster, K., Woda, A., Peyron, M., 2006. Effect of texture of plastic and elastic model foods on the parameters of mastication. Journal of Neurophysiology (95), 3469–3479.

Humphrey, J., 2002. Cardiovascular Solid Mechanics. Cells, Tissues, and Organs. Springer, New York.

Hunter, P., Borg, T., 2003. Integration from proteins to organs: the physiome project. Nature Reviews Molecular Cell Biology 4 (3), 237–243.

Hunter, P., Pullan, A., Smaill, B., 2003. Modelling total heart function. Annual Review Biomedical Engineering 5, 147–177.

Ichim, I., Swain, M., Kieser, J., 2006. Mandibular biomechanics and development of the human chin. Journal of Dental Research 85 (7), 638–642.

Kim, D., Gilson, W.D., Kramer, C.M., Epstein, F.H., 2004. Myocardial tissue tracking with two-dimensional cine displacement-encoded MR imaging: development and initial evaluation. Radiology 230 (3), 862–871.

Koolstra, J., van Eijden, T., 1997a. Dynamics of the human masticatory muscles during a jaw open–close movement. Journal of Biomechanics 30 (9), 883–889.

Koolstra, J., van Eijden, T., 1997b. The jaw open–close movements predicted by biomechanical modelling. Journal of Biomechanics 30 (9), 943–950.

Koolstra, J., van Eijden, T., 2001. A method to predict muscle control in the kinematically and mechanically indeterminate human masticatory system. Journal of Biomechanics 34 (9), 1179–1188.

Koolstra, J., van Eijden, T., 2005. Combined finite-element and rigid-body analysis of human jaw joint dynamics. Journal of Biomechanics 38 (12).

Koolstra, J., van Eijden, T., 2006. Prediction of volumetric strain in the human temporomandibular joint cartilage during jaw movement. Journal of Anatomy 209 (3), 369–380.

Koolstra, J., van Eijden, T., Weijs, W., Naeije, M., 1988. A three-dimensional mathematical model of the human masticatory system predicting maximum possible bite forces. Journal of Biomechanics 21 (7), 563–576.

Koolstra, J., van Eijden, T., Weijs, W., 1989. An iterative procedure to estimate muscle lines of action in vivo. Journal of Biomechanics 22 (8-9), 911–920.

Koolstra, J., van Eijden, T., van Spronsen, P., Weijs, W., Valk, J., 1990. Computer-assisted estimation of lines of action of human masticatory muscles reconstructed in vivo by means of magnetic resonance imaging of parallel sections. Archives of Oral Biology 35 (7), 549–556.

Korioth, T.W.P., Romilly, D.P., Hannam, A.G., 1992. Three-dimensional finite element stress analysis of the dentate human mandible. American Journal of Physical Anthropology 88 (1), 69–96.

Lemos, R., Rocke, J., Baranoski, G., Kawakami, Y., Kurihara, T., 2005. Modeling and simulating the deformation of human skeletal muscle based on anatomy and physiology. Computer Animation and Virtual Worlds 16 (3–4), 319–330.

Lund, J., 1991. Mastication and its control by the brain stem. Critical Review of Oral Biology Medicine 2 (1), 33–64.

May, B., Saha, S., Saltzman, M., 2001. A three-dimensional mathematical model of temporomandibular joint loading. Clinical Biomechanics 16 (6), 489–495.

McMillan, A., Hannam, A., 1992. Task-related behaviour of motor units in different regions of the human masseter muscle. Archives of Oral Biology 37 (10), 849–857.

Nash, M., Hunter, P., 2000. Computational mechanics of the heart: from tissue structure to ventricular function. Journal of Elasticity 61, 113–141.

Netter, F., 2003. Atlas of human anatomy, third ed. Icon Learning Systems, Teterboro, NJ.

Nielsen, P.M., Grice, I.J.L., Smaill, B.H., Hunter, P.J., 1991. Mathematical model of geometry and fibrous structure of the heart. AJP—Heart and Circulatory Physiology 260, H1365–H1378.

O'Connor, C., Franciscus, R., Holton, N., 2005. Bite force production capability and efficiency in neandertals and modern humans. American Journal of Physical Anthropology 127 (2), 129–151.

Oomens, C.W.J., Maenhout, M., van Oijen, C.H., Drost, M.R., Baaijens, F.P., 2003. Finite element modelling of contracting skeletal muscle. Philosophical Transactions of the Royal Society B: Biological Sciences 358 (1437), 1453–1460.

Pullan, A., Cheng, L., Yassi, R., Buist, M., 2004. Modelling gastrointestinal bioelectric activity. Progress in Biophysics and Molecular Biology 85, 523–550.

Röhrle, O., Foster, K., Waddell, N., Anderson, I., Pullan, A., 2007. Evaluation of the use of a motion-capture technique for chewing trajectories with six degrees of freedom. Journal of Texture Studies, in review.

Sacks, M., Sun, W., 2003. Multiaxial mechanical behaviour of biological materials. Annual Review Biomedical Engineering 5 (251–284).

Spitzer, V., Ackerman, M., Scherzinger, A., Whitlock, D., 1996. The visible human male: a technical report. Journal of the American Medical Informatics Association 3 (2), 118–130.

Tawhai, M., Hunter, P., Tschirren, J., Reinhardt, J., McLennan, G., Hoffman, E., 2004. Ct-based geometry analysis and finite element models of the human and ovine bronchial tree. Journal of Applied Physiology 97 (6), 2310–2321.

Teran, J., Sifakis, E., Blemker, S.S., Ng-Thow-Hing, V., Lau, C., Fedkiw, R., 2005. Creating and simulating skeletal muscle from the visible human data set. IEEE Transactions on Visualization and Computer Graphics 11 (3), 317–328.

Throckmorton, G., 1985. Quantitative calculations of temporomandibular joint reaction forces—ii. The importance of the direction of the jaw muscle forces. Journal of Biomechanics 18 (6), 453–461.

van Eijden, T., Korfage, J., Brugman, P., 1997. Architecture of the human jaw-closing and jaw-opening muscles. The Anatomical Record 248, 464–474.

van Essen, N., Anderson, I., Hunter, P., Carman, J., Clarke, R., Pullan, A., 2005. Anatomically based modelling of the human skull and jaw. Cells Tissues Organs 180 (1), 44–53.

van Loon, J., Otten, E., Falkenstrom, C., de Bont, L., Verkerke, G., 1998. Loading of a unilateral temporomandibular joint prosthesis: a three-dimensional mathematical study. Journal of Dental Research 77 (11), 1939–1947.

Weijs, W., Hillen, B., 1985. Cross-sectional areas and estimated intrinsic strength of the human jaw muscles. Acta Morphologica Neerlando-Scandinavica 23 (3), 267–274.

Yucesoy, C., Koopman, B., Baan, G., Grootenboer, H., Huijing, P., 2003. Effects of inter- and extramuscular myofascial force transmission on adjacent synergistic muscles: assessment by experiments and finite-element modeling. Journal of Biomechanics 36 (12), 1797–1811.